ACS Partner Journal

CHEMICAL & BIOMEDICAL IMAGING

Editors' Choice

Open Access

pubs.acs.org/ChemBioImaging

Article

Non-Small Cell Lung Cancer Imaging Using a Phospholipase A2 Activatable Fluorophore

Michael C. Hart,[†] Ritesh K. Isuri,[†] Drew Ramos, Sofya A. Osharovich, Andrea E. Rodriguez, Stefan Harmsen, Grace C. Dudek, Jennifer L. Huck, David E. Holt, Anatoliy V. Popov, Sunil Singhal, and Edward J. Delikatny*

Cite This: *Chem. Biomed. Imaging* 2024, 2, 490−500

Read Online

ACCESS | Metrics & More | Article Recommendations | Supporting Information

ABSTRACT: Lung cancer, the most common cause of cancer-related death in the United States, requires advanced intraoperative detection methods to improve evaluation of surgical margins. In this study we employed DDAO-arachidonate (DDAO-A), a phospholipase A2 (PLA2) activatable fluorophore, designed for the specific optical identification of lung cancers in real-time during surgery. The *in vitro* fluorescence activation of DDAO-A by porcine sPLA2 was tested in various liposomal formulations, with 100 nm extruded EggPC showing the best overall characteristics. Extruded EggPC liposomes containing DDAO-A were tested for their stability under various storage conditions, demonstrating excellent stability for up to 4 weeks when stored at −20 °C or below. Cell studies using KLN 205 and LLC1 lung cancer cell lines showed DDAO-A activation was proportional to cell number. DDAO-A showed preferential activation by human recombinant cPLA2, an isoform highly specific to arachidonic acid-containing lipids, when compared to a control probe, DDAO palmitate (DDAO-P). *In vivo* studies with DBA/2 mice bearing KLN 205 lung tumors recapitulated these results, with preferential activation of DDAO-A relative to DDAO-P following intratumoral injection. Topical application of DDAO-A-containing liposomes to human (n = 10) and canine (n = 3) lung cancers *ex vivo* demonstrated the preferential activation of DDAO-A in tumor tissue relative to adjacent normal lung tissue, with fluorescent tumor-to-normal ratios (TNR) of up to 5.2:1. The combined results highlight DDAO-A as a promising candidate for clinical applications, showcasing its potential utility in intraoperative and back-table imaging and topical administration during lung cancer surgeries. By addressing the challenge of residual microscopic disease at resection margins and offering stability in liposomal formulations, DDAO-A emerges as a potentially valuable tool for advancing precision lung cancer surgery and improving curative resection rates.

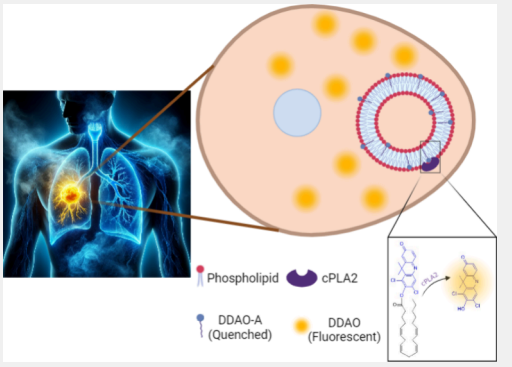

KEYWORDS: *non-small cell lung carcinoma, fatty acids, activatable fluorescent probes, imaging agents, liposomes*

INTRODUCTION

Lung cancer is the leading cause of cancer-related death in the United States, with a 5-year survival rate of less than 20%. Lung cancers encompass small cell lung cancer (SCLC) and non-small cell lung cancer (NSCLC), with NSCLCs accounting for approximately 85% of all cases. NSCLC can be further categorized into adenocarcinomas, squamous cell carcinomas, and large cell undifferentiated carcinomas.[1−3] The primary treatment for NSCLCs is surgery followed by adjuvant chemotherapy.[3,4] The current intraoperative identification of tumor tissue and delineation of margins relies primarily on finger palpation and visual inspection. However, these conventional approaches lack specificity, resulting in disease recurrence in approximately 40% of patients.[4−6]

Preoperative imaging offers essential information on tumor localization and nodule count. However, during surgery, the lung is collapsed so there is an inherent shift in the organ position compared to presurgical imaging which poses challenges for accurate tumor margin delineation during resection. Furthermore, the need to preserve lung function in patients with compromised respiratory systems requires conservative tissue removal, increasing the risk of residual disease in the lungs. Thus, there is an urgent need for the development of specific intraoperative imaging and tumor identification methods to enhance the rates of successful curative resections.

Fluorescence-guided surgery (FGS) is an emerging field aimed at addressing this issue by utilizing fluorophores targeted at tumors, disease biomarkers, or cell types to identify tumor margins and micrometastases intraoperatively.[7−12] By

Received: March 7, 2024
Revised: April 25, 2024
Accepted: April 29, 2024
Published: June 20, 2024

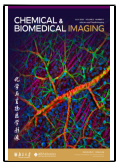

targeting overexpressed disease biomarkers and exploiting the enhanced permeability and retention (EPR) effect, fluorophores can be designed to preferentially partition into specific tissues. Such probes can be invaluable for achieving complete malignant tissue resections and for visualizing healthy tissues such as nerves, thereby reducing the rates of disease recurrence and postoperative complications.[13,9,14−17] Despite being a nascent technology, FGS holds substantial promise. However, only a limited number of fluorescent probes have received clinical approval, and only a few are specifically designed for cancer imaging, such as ICG, 5-aminolevulinic acid (5-ALA), and pafolacianine (OTL-38).[15,18−21] There is considerable interest in developing near-infrared (NIR) fluorophores for FGS. At these longer wavelengths, tissue light penetration is increased and scattering is reduced relative to visible light.[7−9,18−20,22]

Activatable fluorophores have been devised to enhance fluorescence signal intensity by increasing probe accumulation at sites of high target expression. The use of enzyme-activaated probes has demonstrated the potential to increase signal-to-background ratios (SBR) by as much as 10-fold compared to constitutively active fluorophores.[23−29]

We previously reported a NIR-I phospholipase A2 (PLA2) activatable fluorophore, DDAO-arachidonate (DDAO-A Supporting Information Scheme S1), for the targeted imaging of triple-negative breast cancer (TNBC).[30,31] DDAO-A is composed of the fluorophore DDAO (*7-hydroxy-9H(1,3-dichloro-9,9-dimethylacridin-2-one*)) conjugated to arachidonic acid through an ester linkage, effectively quenching fluorescence.[30,32,33] DDAO-A must be formulated into liposomes due to the hydrophobicity of the probe. When DDAO-A-containing liposomes are exposed to PLA2 activity, the ester linkage is cleaved resulting in free DDAO (λ_{ex}, λ_{em} = 600, 660 nm) with measurable fluorescence in the NIR-I window.[30,31]

Cytosolic PLA2 (cPLA2) is a highly selective PLA2 isoform that catalyzes the release of arachidonic acid from phospholipids for inflammation signaling and is overexpressed in approximately 45% of non-small cell lung cancers (NSCLCs).[34,35] Additionally, cPLA2 is activated by phosphorylation through the Ras/Raf/MAPK pathway, which has well-documented mutations in as many as 30% of NSCLC adenocarcinomas alone.[36,37]

In translating this probe from TNBC imaging to NSCLC, we hypothesized that DDAO-A would be preferentially activated in NSCLCs compared to normal lung tissue due to the overexpression and increased activation of cPLA2 in NSCLC, as well as the increased density of lung cancer tissue. As a result, we expected to observe a strong contrast between malignant and normal tissues that could be translatable for intraoperative and *ex vivo* tumor margin identification. Here, we demonstrate the preferential activation of DDAO-A *in vitro* and *in vivo* NSCLC cells and animal models, as well as in *ex vivo* human (n = 10) and canine (n = 3) lung tumor tissues.

MATERIALS AND METHODS

All reagents for chemical synthesis were obtained from Santa Cruz Biotechnology. Chloroform, hexanes, salts for buffers, and cell culture supplies were purchased from ThermoFisher Scientific unless otherwise stated. Tris base was purchased from Bio-Rad. Lipids for liposomal formulations and materials for membrane extrusion were obtained from Avanti Polar Lipids. Porcine pancreas pancreatic secretory phospholipase A2 (sPLA2) was purchased from MilliporeSigma. Recombinant human cPLA2 was obtained from Abcam. All cell lines were purchased from the American Type Culture Collection (ATCC), unless specified otherwise. Normal human parathyroid and prostate tissues were purchased from OriGene. Mice were purchased from Charles River Production. The rabbit primary antibody for cPLA2 was purchased from Cell Signaling Technologies.

Ethical Statements

Mouse Studies. Ethical approval for the use of mice in this study was obtained and monitored under the Institutional Animal Care and Use Committee (IACUC) through the University of Pennsylvania; Protocol #: 804641.

Canine Tissue Studies. Informed consent for the use of all canine tissues was obtained through the University of Pennsylvania School of Veterinary Medicine, and ethical approval was obtained and monitored under the IACUC through the University of Pennsylvania; Protocol #: 804435.

Human Tissue Studies. Informed consent for the use of all human tissues was obtained through the Hospital of the University of Pennsylvania with ethical approval and monitoring through Internal Review Boards (IRB): 822153 and 842586.

Chemical Synthesis

DDAO-arachidonate (DDAO-A, **3**) and DDAO-palmitate (DDAO-P, **5**) were synthesized as previously reported.[30] Briefly 25 mg (0.081 mmol) of DDAO (**1**) were dissolved in 75 mL of anhydrous pyridine (Millipore Sigma) (Scheme S1). The solution was cooled to −40 °C by swirling in a liquid N_2 bath. 100 mg (0.310 mmol) of arachidonoyl chloride (**2**) or 90.6 mg (0.330 mmol) of palmitoyl chloride (**4**, Sigma-Aldrich) were then added to the solution and stirred until the solution equilibrated to room temperature (Scheme S1). Pyridine was removed by rotary evaporation at rt. The resulting solids were reconstituted in 1:1 (v:v), hexanes:chloroform and purified by flash column chromatography (silica gel, porosity 60 Å, particle size 40−63 μm, Sorbent Technologies) in 100 mL gradients of 3:7, 2:8, 1:9 (v:v), hexanes:chloroform followed by 100 mL of pure chloroform. Yellow solids were obtained by rotary evaporation followed by high vacuum drying to remove residual solvents. Yields: DDAO arachidonate 32.2 mg (67%); DDAO palmitate 21.8 mg (49%). The purified products were confirmed by mass spectroscopy (MALDI-TOF)[30] and ^{1}H NMR.[30]

Liposomal Formulation

Egg phosphatidylcholine (EggPC) liposomes were prepared to be 95:5 mol % EggPC:DDAO-A by combining 1.9 μmol EggPC with 0.1 μmol DDAO-A in chloroform. EggPC-cholesterol liposomes were prepared to be 52:43:5 mol % EggPC:cholesterol:DDAO-A in chloroform by combining 1.05 μmol EggPC with 0.85 μmol cholesterol and 0.1 μmol DDAO-A in chloroform. Hydrogenated soybean phosphatidylcholine (HSPC) 1,2-distearoyl-*sn*-glycero-3-phosphoethanolamine-N-[amino(polyethylene glycol)-2000] (DSPE-PEG2000) liposomes were formulated to be 50:40:5:5 mol %, HSPC:cholesterol:DSPE-PEG2000:DDAO-A by combining 1 μmol HSPC, 0.8 μmol cholesterol, 0.1 μmol DSPE-PEG2000, and 0.1 μmol DDAO-A in chloroform. DDAO-P was similarly dissolved in chloroform and combined with the desired lipid composition. Chloroform was removed under a constant stream of N_2 gas creating lipid films. The films were reconstituted in 1.0 mL Dulbecco's phosphate buffered saline (DPBS) by vigorous pipetting and vortexing. Membrane extrusion was performed using the Avanti Mini Extruder. Liposomes were extruded 20 times across a 50, 100, or 200 nm membrane.

Liposomal Characterization

Absorbance and fluorescence spectra were acquired using a Molecular Devices SpectraMax M5. Reference absorbances were acquired for the solvent before the addition of the probe. Absorbance spectra for DDAO-A- and DDAO-A-containing liposomes were obtained by measuring the absorbance every 1 nm from 300 to 850 nm and normalizing to the wavelength with the highest absorption. Absorbance spectra for DDAO-A were obtained in 3 mL of chloroform using a quartz cuvette. Spectra for DDAO-A liposomes

https://doi.org/10.1021/cbmi.4c00026
Chem. Biomed. Imaging 2024, 2, 490−500

were determined in 100 μL of DPBS at pH 9.0 in a Costar 96-well black wall clear bottom plate.

Size and polydispersity indices (PDIs) of liposomes for each formulation were determined using dynamic light scattering (DLS), and Zeta potentials were determined by electrophoretic light scattering (ELS). All characterization experiments were run in triplicate in 0.1X PBS on the Malvern Panalytical Zetasizer.

To test the stability of EggPC-DDAO-A lipid films, the films were stored under N_2 gas at room temperature with ambient light or in the dark covered in aluminum foil at room temperature, 4 °C, −20 °C, and −80 °C. After 1 day, 2 days, 7 days, 14 days, and 28 days, lipid films were used to formulate liposomes as described above. The amount of remaining DDAO-A, as well as, the amount of DDAO released by nonspecific hydrolysis, was assessed by measuring absorbance and fluorescence spectra, respectively.

Cell Culture

Lewis lung carcinoma (LLC1), LKR and KLN 205 cells were obtained from ATCC. 4175-Luc+ cells were obtained from Dr. Andy Minn. TC1 cells were generously provided by Dr. Sunil Singhal. Frozen stocks were maintained in liquid nitrogen cryogenic storage. Cells were tested every 6 months using the MycoAlert mycoplasma testing kit (Lonza). LLC1 and LKR cells were passaged in full Gibco high glucose (4.5 g/L) DMEM. KLN 205 cells were passaged using full EMEM from ATCC. TC1 cells were passaged using folate-deficient RPMI (Mediatech). 4175-Luc+ cells were passaged in DMEM supplemented with 5 μg/mL blasticidin (Invitrogen). All media were supplemented with 10% fetal bovine serum (FBS) (Hyclone), 1% L-glutamine (Gibco), and 1% penicillin/streptomycin (Gibco).

Western Blot

Cells were seeded in 10 cm dishes at 2.5×10^5 cells/mL in 12 mL of media. After incubation for 24 h at 37 °C and 5% CO_2, cells were washed with ice-cold DPBS and scraped on ice in radioimmunoprecipitation assay buffer containing complete, mini EDTA-free protease inhibitor cocktail (Roche). The resulting samples were vortexed and rapidly frozen and thawed in three cycles using liquid N_2 followed by heating in a 37 °C heat block. Samples were then sonicated for 5 min at 4 °C and kept on ice for 15 min. Cell debris was pelleted by centrifugation at 13,000 rpm for 10 min. The supernatant was removed, and protein concentration measured using a bicinchonic acid (BCA) protein assay kit (Pierce). Protein concentrations were equalized before diluting 1:1 with Laemmli loading buffer containing 5% 2-mercaptoethanol and heating for 5 min at 95 °C. Thirty μL (25 μg protein) were loaded into each lane for each corresponding cell line and resolved on a 10% SDS-PAGE gel. Transfer was conducted onto a 0.45 μm pore nitrocellulose membrane (Invitrogen). The membrane was blocked in Odyssey blocking buffer (LI-COR) and incubated with primary antibodies to cPLA2 and β-tubulin (Cell Signaling). The membrane was incubated with secondary goat anti-rabbit antibody conjugated to IRDye 800CW (LI-COR) and visualized using the LI-COR Odyssey CLx. Bands were quantified using ImageStudio Lite.

Activation Assays

For detecting activation by sPLA2, 100, 50, 10, or 0 units of the enzyme were added in triplicate to each well of a Costar 96-well black wall clear bottom plate. One nmol of liposomal DDAO-A or DDAO-P was added to each well to start the assay. Reactions were conducted in 100 μL total volume DPBS. To test fluorescence activation by cPLA2, 2 nmol of liposomal DDAO-A or DDAO-P were incubated with 2.5−5 μg of recombinant human cPLA2 or with no enzyme. The reaction volume was made uniform at 100 μL using a 50 mM Tris, 500 mM NaCl and 10 mM $CaCl_2$ buffer (pH = 8). Reactions were conducted at 37 °C. Probe activation was monitored by measuring DDAO fluorescence at 660 nm using a 600 nm excitation in the Molecular Devices SpectraMax M5 plate reader.

KLN 205 cells were seeded in duplicates in a Nunc Lab-Tek II 8-well Chamber Slide System at 0, 1.5×10^5 or 3.0×10^5 cells/mL in a total volume of 200 μL EMEM. LLC1 cells were seeded in triplicate into a 96-well plate at 0, 1.5×10^5 or 3.0×10^5 cells/mL in a total volume of 100 μL DMEM. Cells were incubated overnight at 37 °C and 5% CO_2. Media was aspirated and replaced with 200 or 100 μL of supplement-free media containing 10 μM DDAO-A in EggPC liposomes and incubated at 37 °C and 5% CO_2 for 3.5 h. Media was aspirated, and wells were rinsed twice with ice-cold DPBS before imaging for fluorescence at 700 nm using the LI-COR Odyssey for the chamber slides or the LI-COR Pearl for the 96-well plate. Fluorescence was quantified for each sample using ImageStudio Lite.

In Vivo Imaging

Eight DBA/2 mice (Charles River) were injected in the shoulder with 1×10^6 KLN 205 cells in 100 μL of 1:1 (v:v) Matrigel Matrix:DPBS. Tumors were allowed to grow for 2 weeks to be about 1 cm^2. The mice were imaged for baseline autofluorescence in the LI-COR Pearl Trilogy at 700 nm. This was followed by three rounds of successive imaging. For experiment 1, four mice were injected intratumorally (IT) with 40 nmol of DDAO-A. Four mice were injected IT with 40 nmol of DDAO-P as negative controls. The probes were allowed to activate for 5 min prior to imaging at 700 nm. In experiment 2, two of the mice injected with DDAO-P were chased with 40 nmol of DDAO-A IT, and the mice were imaged 5 min postadministration at 700 nm. In experiment 3, the remaining two control mice were chased IT with 40 nmol of DDAO-A. Fluorescence imaging was repeated. Pretreatment autofluorescence was subtracted from flank fluorescence after each imaging round to determine the Mean Fluorescence Intensity (MFI) for each mouse and normalized to the highest tumor fluorescence intensity. Following the euthanasia of the mice, all tumors were excised and imaged at 700 nm in the LI-COR Pearl Trilogy alongside flank muscle from the corresponding mice to determine TNR. Fluorescence for all images was quantified using ImageStudio Lite (LI-COR).

Canine and Human Tissue Staining and Imaging

Deidentified canine lung tumor and normal lung tissues were obtained from surgeries in patient dogs with spontaneous lung tumors. Deidentified human lung tumor and normal lung tissues were obtained from lung tumor resection. Fresh tissues were maintained in DPBS on ice for transport and equilibrated to 37 °C prior to treatment. Tissues were imaged for baseline fluorescence at 700 and 800 nm using the LI-COR Pearl or by exciting at 640 nm and measuring emission at 680 nm using the PerkinElmer IVIS Spectrum. The tissues were then placed in 1 mL of DPBS before treating with 20 nmol of liposomal DDAO-A. Samples were incubated at 37 °C for 15 min before reimaging using the same conditions as at baseline. Fluorescence was quantified using ImageStudio Lite (LI-COR) or LivingImage (PerkinElmer), TNRs were determined by dividing the average fluorescence intensity of the tumor by the average fluorescence intensity of the normal tissue.

Histology/Immunohistochemistry

Human and canine tissues from *ex vivo* experiments were placed in 10% paraformaldehyde and stored at room temperature in the dark until needed. Five μm thick paraffin sections were mounted on ProbeOn slides (Thermo Fisher Scientific). Immunostaining was performed using a Leica BOND RXm automated platform combined with the Bond Polymer Refine Detection kit. After dewaxing and rehydration, sections were pretreated with the epitope retrieval BOND ER2 high pH buffer (Leica) for 20 min at 98 °C. Endogenous peroxidases were inactivated with 3% H_2O_2 for 10 min at room temperature. Nonspecific tissue-antibody interactions were blocked with Leica PowerVision IHC/ISH Super Blocking solution for 30 min at room temperature. The blocking solution also served as a diluent for the rabbit primary antibody against cPLA2 (Cell Signaling Technology) at a concentration of 1:200 and incubated on the sections for 45 min at room temperature. A biotin-free polymeric IHC detection system consisting of HRP-conjugated goat anti-rabbit IgG was then applied for 25 min at room temperature. Immunoreactivity was revealed with the diaminobenzidine (DAB) chromogen reaction. The resulting slides were counterstained in hematoxylin, dehydrated in an ethanol series, cleared in xylene, and permanently mounted with

https://doi.org/10.1021/cbmi.4c00026
Chem. Biomed. Imaging 2024, 2, 490−500

a resinous mounting medium (Thermo Scientific ClearVue coverslipper). Sections of normal canine and human parathyroid and prostate were included as positive and negative controls, respectively.

Limit-of-Detection

Human lung tumor tissue was imaged whole and following each of multiple dissections for fluorescence at 700 nm using the LI-COR Pearl Trilogy. Normal human lung tissue from the same patient was imaged alongside each tumor dissection at its original size. TNRs were then determined for each dissection using ImageStudio Lite. Imaging areas for each dissection were determined by measuring the length and width of tumors in each dissection. Imaging area was compared to the TNR for each dissection.

RESULTS AND DISCUSSION

To determine the optimal liposomal formulation for *in vitro*, *in vivo*, and *ex vivo* studies, four different formulations were tested for size, PDI, and zeta potential (Table 1, Figure S1).

Table 1. Physical Characteristics of DDAO-A Liposomes

Formulation[a]	Size (nm)	PDI[b]	Zeta Potential (mV)
EggPC	809.3	0.258	−8.47 ± 1.2
100 nm EggPC	105.7	0.094	−15.13 ± 2.4
55:45 EggPC:Cholesterol	109.1	0.093	−12.9 ± 8.14
100 nm HSPC	100.1	0.087	−17.20 ± 3.6

[a]**EggPC** = L-α-egg phosphatidylcholine:DDAO-A, 95:5 mol %. **HSPC** = Hydrogenated soybean phosphatidylcholine:cholesterol:1,2-distearoyl-*sn*-glycero-3-phosphoethanolamine-polyethylene glycol 2000:DDAO-A, 50:40:5:5 mol %. [b]**PDI** = Polydispersity index.

Nanoparticles measuring less than 200 nm partition preferentially into cancer tissues via the EPR effect.[38−40] Thus, developing a formulation with sizes around 100 nm and low PDIs was important for ensuring experimental reproducibility and maximizing tumor tissue accumulation. Zeta potentials were considered optimal within the range of −5 to −15 mV. Within this interval the liposomes bear a sufficiently negative charge to minimize interliposomal fusion, while still retaining a low enough charge to enhance *in vivo* liposomal retention by reducing cellular fusion.[38,41] Among the four formulations tested, only two exhibited the desired physical characteristics: membrane-extruded EggPC liposomes and 55:45 EggPC:cholesterol liposomes (Table 1). Nonextruded EggPC liposomes displayed varying sizes with their average liposomal size being nearly four times larger than the optimal size, whereas the Zeta potential for the HSPC liposomal formulation was below −15 mV (Table 1, Figure S1).

All four formulations were evaluated for their activation by sPLA2, a less specific isoform that cleaves phospholipids during digestion to release various fatty acids, including arachidonic and palmitic acids.[42−44] The activation of DDAO-A in each liposomal formulation was tested using 0−100 units of porcine pancreas sPLA2 (Figure 1). Nonextruded and membrane-extruded EggPC liposomes exhibited the most rapid activation of DDAO-A and the highest overall fluorescence after 3.5 h. These formulations displayed distinguishable fluorescence proportional to the enzyme concentration as early as 30 min following reaction initiation (Figure 1**A**,**B**). The addition of cholesterol to the EggPC formulation resulted in slower activation and a lower maximum fluorescence which was reached at 10 h (Figure 1C). HSPC liposomes exhibited virtually no activation of DDAO-A in the presence of any amount of sPLA2 (Figure 1D).

The primary purpose of this probe is for imaging lung cancer margins following topical administration during surgical resections or for back table imaging of surgical specimens, thus rapid activation is needed to ensure its surgical utility. Fluorescence imaging of tumors *ex vivo* relies on the rapid uptake and activation of the fluorophore to assess positive tumor margins. Thus, the kinetics of DDAO-A were critical in determining the formulation to be used in later studies. The maximum fluorescence of 55:45 EggPC:cholesterol liposomes was notably below the maximum observed in membrane-extruded EggPC liposomes. Due to the combination of the high fluorescence signal at maximum activation and the optimal physical properties, membrane-extruded EggPC liposomes were selected for use in future experiments. While the other liposomal formulations showed little promise as DDAO-A carriers *in vitro*, the HSPC or 55:45 EggPC:cholesterol formulation may be useful for *in vivo* systemic administration due to the increased circulation times associated with cholesterol-containing liposomes, allowing for increased partitioning to the tumor and tumor microenvironment prior to activation.[45,46]

EggPC lipid films formulated with DDAO-A were assessed for stability under different storage conditions. Lipid films were stored at temperatures ranging from −80 °C to room temperature (RT) for up to 28 days, with and without light

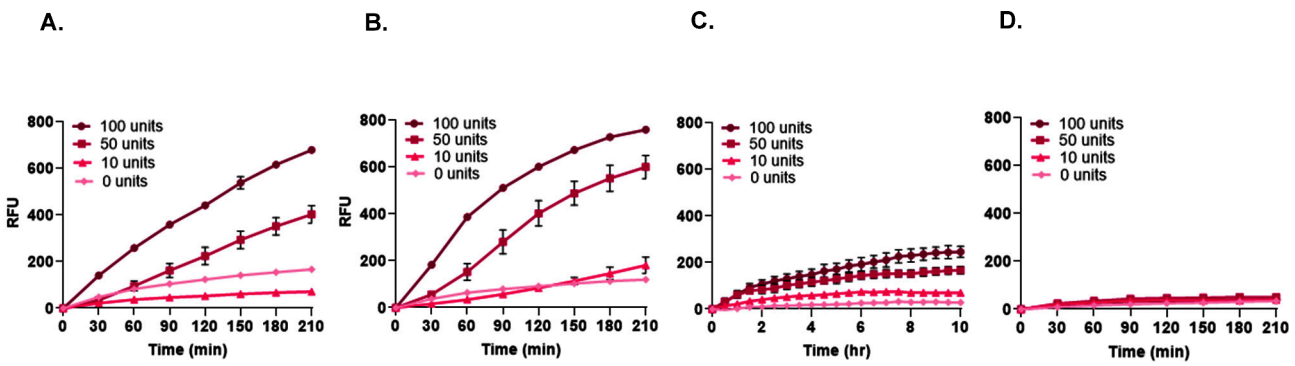

Figure 1. Fluorescence activation of DDAO-A in various liposomal formulations using sPLA2. A. EggPC liposomes without membrane extrusion exhibited strong activation of DDAO-A by sPLA2 within 30 min. **B**. 100 nm membrane-extruded EggPC liposomes exhibited strong activation of DDAO-A by sPLA2 within 30 min. **C**. 100 nm membrane-extruded 55:45 EggPC:Cholesterol liposomes demonstrated slow fluorescence activation of DDAO-A. Maximum fluorescence was reached at 10 h postreaction initiation. **D**. 100 nm membrane-extruded HSPC liposomes showed almost no activation of DDAO-A by sPLA2.

https://doi.org/10.1021/cbmi.4c00026
Chem. Biomed. Imaging 2024, 2, 490−500

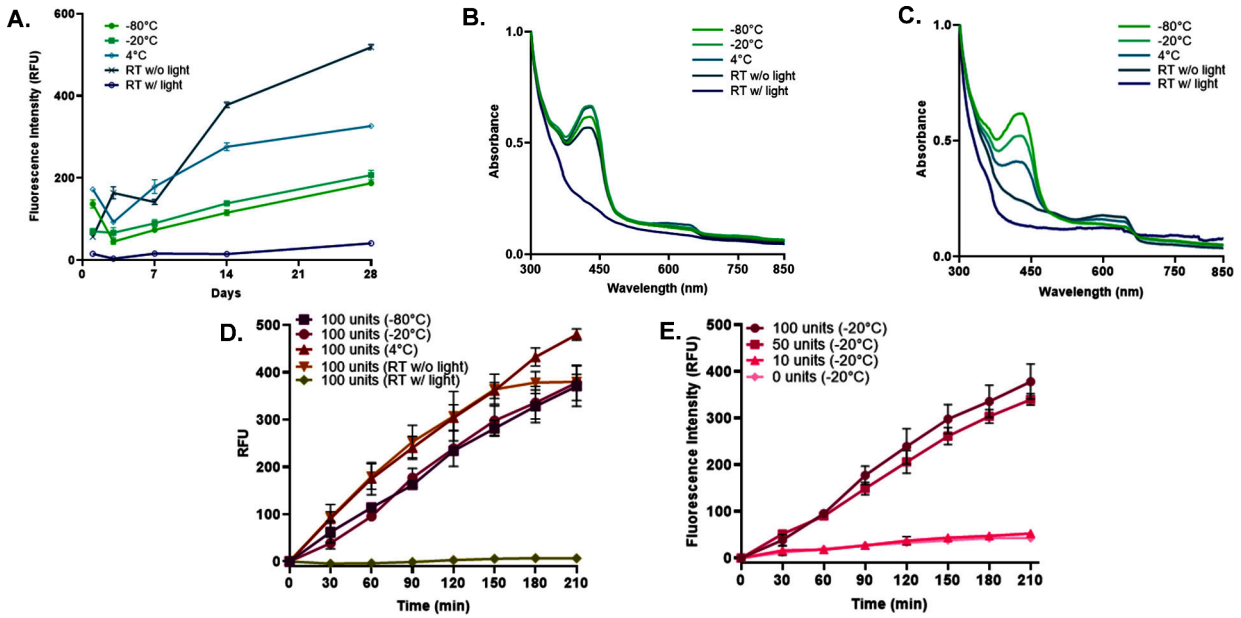

Figure 2. Effects of storage temperature on DDAO-A lipid film stability. **A**. Initial fluorescence of liposomes as a function of time following storage at different temperatures and light exposures. **B**. Absorbance spectra of liposomes after 1 day under various storage conditions. Absorbance peaks at 430 nm were indicative of intact DDAO-A. **C**. Absorbance spectra of liposomes after 28 days under various storage conditions. The absorbance of free DDAO at 600 nm increased as a function of time and with increasing storage temperatures. **D**. Fluorescence activation of liposomes after 4 weeks of storage when incubated with 100 units of sPLA2. **E**. Fluorescence activation by low concentrations of sPLA2 was distinguishable from higher concentrations after 4 weeks storage at −20 °C.

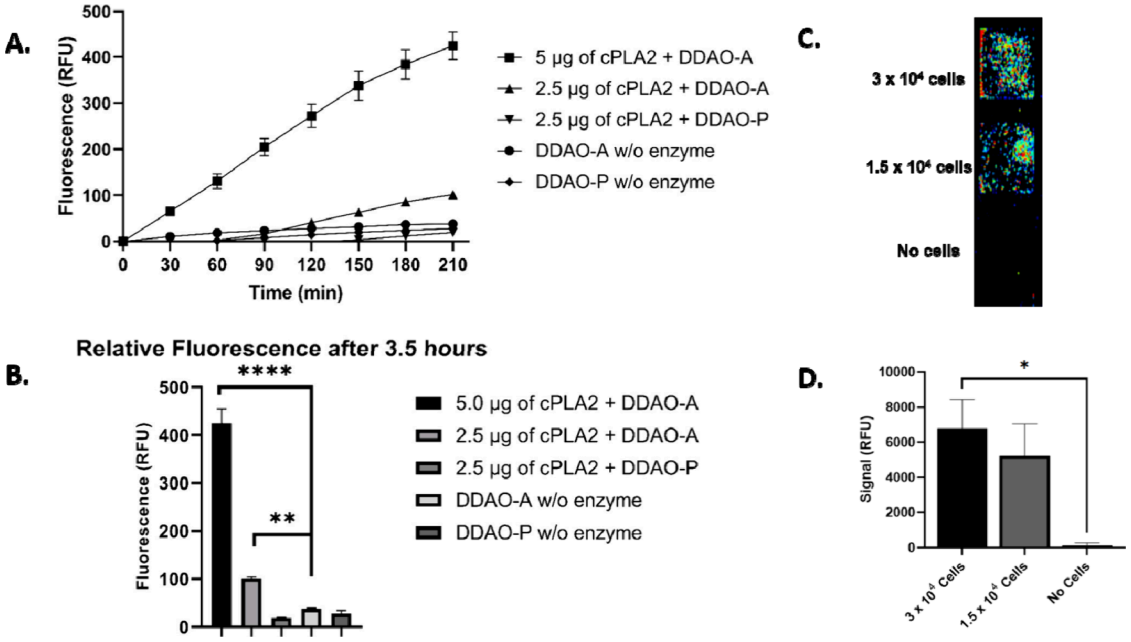

Figure 3. DDAO-A activation by recombinant cPLA2 and KLN 205 cells. **A**. Recombinant human cPLA2 specifically activated DDAO-A compared to DDAO-P or nonspecific aqueous hydrolysis when no enzyme was present. **B**. Quantification of the fluorescence after 3.5 h. DDAO-A exhibits high fluorescence in a concentration dependent manner. DDAO-P shows no significant fluorescence as compared to the control. **C**. KLN 205 cells exhibited significantly increased activation of DDAO-A. **D**. Quantification of the cellular fluorescence from KLN 205 showed a significant dependence on cell number. Unpaired *t* tests (*p-value <0.05, **p-value <0.01, ****p-value <0.0001).

exposure, and were regularly tested for initial absorbance and fluorescence of liposomes, as well as fluorescence resulting from activation by sPLA2 (Figure 2, Figures S2, S3). Light exposure at ambient temperature resulted in rapid photobleaching of the lipid film, as demonstrated by low initial fluorescence at all time points (Figures 2**A**, S3). Additionally, the light-exposed lipid film exhibited no fluorescence activation in the presence of sPLA2 or in the absence of the enzyme (Figures 2D, S3). When lipid films were stored in the dark, the initial fluorescence of liposomes increased slowly with storage time, correlating with storage temperature (Figure 2A). This indicated slow decomposition over time and at higher temperatures.

https://doi.org/10.1021/cbmi.4c00026
Chem. Biomed. Imaging 2024, 2, 490−500

The absorbance spectra of liposomal DDAO-A has a maxima peak at 430 nm, while free DDAO has a maximum absorbance at 600 nm.[30] A gradual decline in signal at 430 nm was observed over 28 days, with lipid films stored at lower temperatures exhibiting higher absorbance at 430 nm (Figure 2B, C). Additionally, the absorbance of each formulation at 600 nm increased with higher storage temperatures (Figure 2B, C). When stored at temperatures above −20 °C, absorbance at 430 nm decreased while absorbance at 600 nm increased, consistent with nonspecific cleavage of the ester bond and release of free DDAO.

Despite this degradation, films stored at temperatures as high as 4 °C exhibited similar increases in fluorescence as films stored at lower temperatures when incubated with sPLA2. Fluorescence activation was observed for all formulations when incubated with 100 units of sPLA2 except for the light-exposed film, at all time points from Day 1 to Day 28 (Figure 2D, Figures S2, S3). Incubation of liposomes stored at −20 °C with 0−100 units of sPLA2 showed increased fluorescence with high sPLA2 concentrations (50 and 100 units) compared to lower concentrations of the enzyme (0 and 10 units) (Figure 2E). Overall, the data demonstrates that the probe remained viable for assessing activation for at least 28 days after storage at temperatures below 4 °C, with the least probe degradation observed at temperatures of −20 °C or lower.

Formulating liposomes, while not inherently complex, necessitates specialized resources and equipment that may not be readily accessible in clinical settings. Streamlining the formulation process without compromising probe integrity is vital to enhance the probe's accessibility and clinical utility. The formulation of DDAO-A liposomes involved an initial step of combining the probe with lipids in chloroform, followed by solvent evaporation under N2 gas to create a lipid film. Subsequently, reconstitution in PBS and extrusion through a 100 nm membrane were performed. Given the probe's proven stability, we propose that the initial step can be conducted prior to distribution to clinical settings, followed by the use of automated membrane extrusion equipment for reconstituting preprepared lipid films.

The relatively high cost of purified cPLA2 made sPLA2 an economical alternative for early testing of DDAO-A. However, it remained necessary to validate the activation of our probe by the designated target enzyme. To this end, we measured the ability of recombinant human cPLA2 to activate both DDAO-A and DDAO-Palmitate (DDAO-P) *in vitro*. While DDAO-A has demonstrated the ability to be activated by multiple phospholipase A2 isozymes, including cPLA2 and sPLA2, it is important to note that the control probe, DDAO-P, exhibits lower sensitivity to cPLA2 due to this enzyme's specificity for lipids containing arachidonic acid.[30,31,47] DDAO-A exhibited a significant increase in fluorescence as early as 30 min postinitiation, with the magnitude of activation being proportional to the concentration of the enzyme (Figure 3A). In contrast, DDAO-P displayed no significant activation by cPLA2 when compared to nonspecific hydrolysis in the absence of the enzyme. Therefore, we confirmed that DDAO-A is indeed activated by the intended target enzyme, cPLA2.

Western blot analysis of cPLA2 expression in TNBC and NSCLC cell lines demonstrated high expression of the target in NSCLC cell lines (Figure S4). Therefore, DDAO-A activation was surveyed in two NSCLC cell lines: KLN 205 and LLC1. Both cell lines exhibited increased fluorescence activation after a 3.5-h incubation with the probe, underscoring the potential of DDAO-A for *ex vivo* NSCLC imaging (Figure 3C,D, S5).

We conducted further assessment of DDAO-A activity using the KLN 205 cell line. KLN 205 cells were incubated for 3-h with either DDAO-A or DDAO-P, followed by costaining with Hoechst nuclear stain. The cells were subsequently analyzed using wide-field fluorescence microscopy (Figure 4). Our

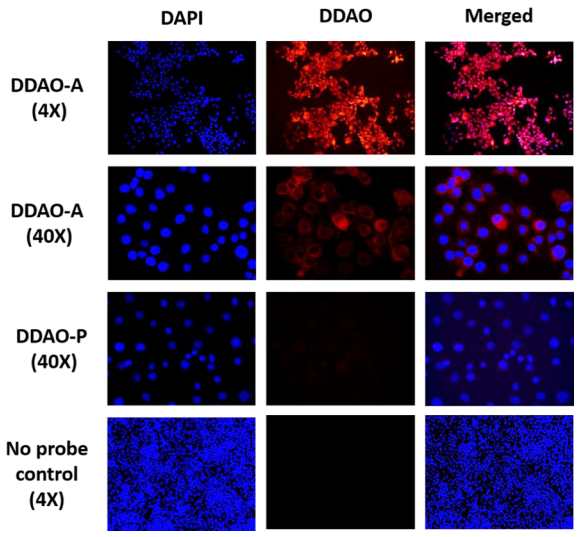

Figure 4. Activation of DDAO-A by KLN 205 cells. KLN 205 cells were incubated with DDAO-A or DDAO-P for 3 h. Wide field fluorescent microscopy was used to visualize free DDAO fluorescence. Nuclei were counterstained with Hoechst dye. Separate and merged fluorescence images are shown with pink showing overlap in the merged image. Cells treated with DDAO-A showed increased fluorescence throughout cytoplasm and in the perinuclear region while cells treated with DDAO-P or in the absence of any probe showed no DDAO fluorescence.

observations revealed robust intracellular fluorescence in cells treated with DDAO-A, in stark contrast to the absence of fluorescence in cells exposed to DDAO-P. The fluorescence emanating from DDAO-A displayed a characteristic distribution throughout the cytoplasm, notably featuring a high concentration of fluorescence in the perinuclear region. This observation aligns with the expected subcellular localization of cPLA2 activity and provides further validation of DDAO-A's specificity and effectiveness.[31,48,49]

DBA/2 mice bearing subcutaneous shoulder KLN 205 tumors were injected intratumorally with DDAO-A and DDAO-P, and probe activation imaged to differentiate between sPLA2- and cPLA2-mediated cleavage (Figure 5A, Figure S6). This experiment was conducted to demonstrate the feasibility for local administration of DDAO-A intraoperatively for NSCLC imaging. Mice treated with DDAO-A displayed robust fluorescence at 700 nm as early as 5 min postinjection (Figure 5B, C). Mice injected with DDAO-P showed minimal alterations in fluorescence from baseline. A chase experiment was conducted in which mice treated with DDAO-P were subsequently administered DDAO-A, which led to an increase in tumor fluorescence. After this experiment, tumors were excised and fluorescence was compared *ex vivo* to muscle fluorescence with *ex vivo* TNR ranging from 2.78:1 to 9.47:1 for each tumor (Figure 5D).

In a previous study with TNBC tumor-bearing mice, intravenous administration of DDAO-A and DDAO-P

https://doi.org/10.1021/cbmi.4c00026
Chem. Biomed. Imaging 2024, 2, 490−500

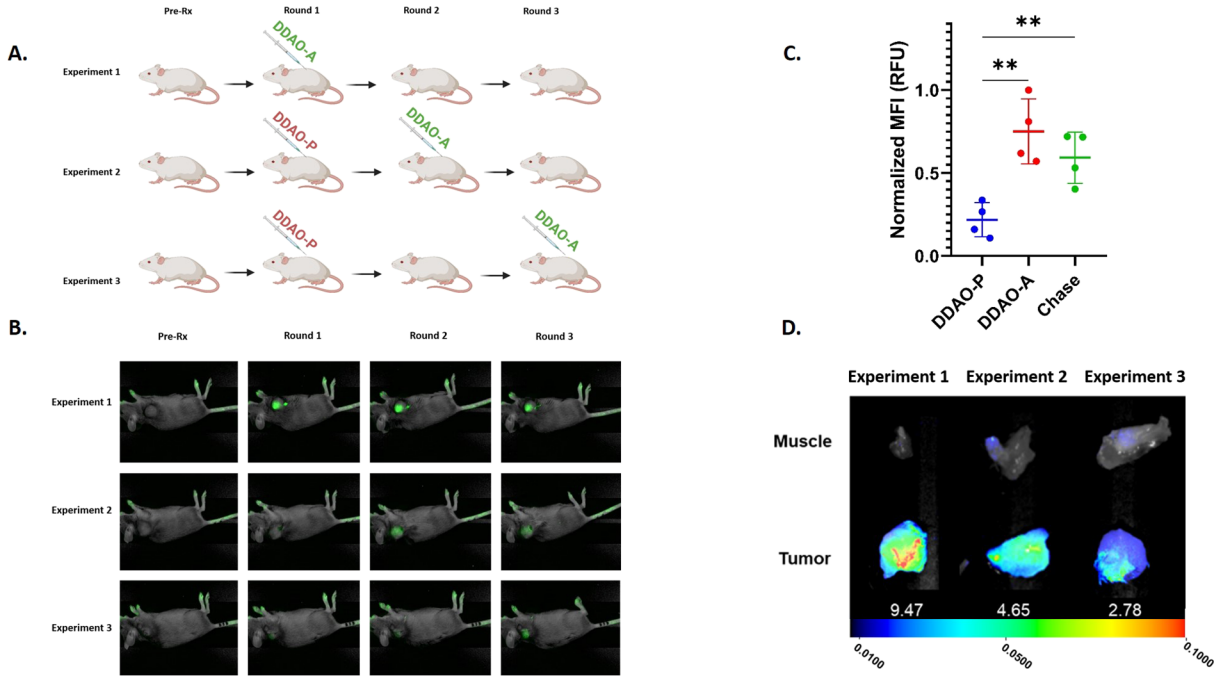

Figure 5. *In vivo* activation of DDAO-A in KLN 205 tumor-bearing mice. **A**. Timeline of study design showing imaging rounds for 3 experiments. Mice were treated with DDAO-A (green) or DDAO-P (red) starting in Round 1 and chased with DDAO-A through Round 3. **B**. Fluorescent images of mice were obtained prior to treatment and at each stage of the study. Tumors treated with DDAO-A exhibited fluorescence within 5 min of injection. Tumors from mice treated with DDAO-P first did not exhibit a strong increase in fluorescence compared to pretreatment (Pre-Rx) fluorescence. Tumor fluorescence was increased in DDAO-P treated mice by subsequent DDAO-A treatment. **C**. Quantified MFI for each mouse ($n = 4$) before and after treatment with DDAO-P, DDAO-A, and following DDAO-A chase of DDAO-P. Signal was defined by tumor margins and compared to background flank fluorescence. Unpaired t test (**p-value <0.01) **D**. Tumor fluorescence *ex vivo* was consistently distinguishable from normal flank muscle tissue fluorescence based on calculated TNRs (in white) for each mouse.

demonstrated limited tumor uptake and activation of the probe, likely attributable to the insufficient circulation time of liposomes.[31] However, the current data have shown that direct administration via intratumoral injection or by topical administration *ex vivo* is effective in identifying tumor tissue using the DDAO-A probe. These findings suggest that DDAO-A has potential as an agent for backbench imaging or topical administration in the surgical cavity.

To further confirm the utility of DDAO-A for back-table imaging, deidentified tissues from canine patients (n = 3) undergoing a clinical trial at the University of Pennsylvania School of Veterinary Medicine for the detection of NSCLC using the NIR-I fluorophore JAS239[50,51] were obtained during surgery and tested for topical DDAO-A activation. Baseline fluorescent images were obtained at 700 nm on the LI-COR Pearl to determine the initial fluorescence of the tissues resulting from systemic administration of JAS239, an NIR-I fluorecent agent developed in our lab (Figure S7). Initial TNRs were determined for each tissue set and compared to the TNRs following immersion in DDAO-A (Figure 6**A**, Table 2). In each case, topical administration of DDAO-A increased the TNR from 1.8, 2.5, and 2.4 to 2.5, 4.6, and 3.5 respectively. TNRs of 2:1 or higher were considered optimal to distinguish between tumor and normal tissues. Hematoxylin and eosin (H&E) staining of the tissues was conducted to confirm the tissue identification as tumor or normal. IHC staining for cPLA2 was conducted in normal lung and lung tumor samples and showed qualitatively higher expression in lung tumor tissues for all three specimens (Figure 5B).

Deidentified human lung tumor and normal lung tissues (n = 10) were obtained during surgeries at the Hospital of the University of Pennsylvania, and assessed for their ability to activate DDAO-A with topical application. Most of the tissues came from patients with early- to midstage adenocarcinomas and were evenly distributed between male and female patients (Table 3). All tissue sets except one were obtained fresh. The remaining tissue set was retrieved from −80 °C storage, 18 months postresection. Fluorescence was measured at 700 nm following treatment with DDAO-A. Preferential activation of DDAO-A by tumor tissues was observed in all tissue sets (Figure 6**C**, S8); 8 out of 10 tissue sets had fluorescent TNRs of 2:1 or higher (Table 3, Figure S8). Hematoxylin and eosin staining followed by IHC for cPLA2 expression was conducted for the tissue sets to confirm tissue identification. cPLA2 expression was qualitatively higher in tumor tissues than normal lung tissues (Figure 6**D**, Figure S9).

In 8 out of the 10 human tissue sets and in all canine tissue sets treated with DDAO-A, tumor fluorescence at 700 nm was at least 2-fold greater than the associated normal tissues. These data indicate that DDAO-A is a strong candidate for delineating lung tumor from normal lung tissues and could be useful in back-table imaging for identifying positive tumor margins in freshly resected specimens. By employing a targeted imaging agent for lung tumors, surgeons will be able to improve intraoperative identification and total resection of NSCLC lesions compared to relying on nonspecific detection such as tissue palpation and visual inspection.

Notably, one of the tumor and normal lung tissue sets was frozen at −80 °C for 18 months. DDAO-A activation was tested in these tissues following thawing and equilibrating to 37 °C (Figure 6**C**). The observed TNR was 2.9:1 showing preferential activation of DDAO-A in the lung tumor tissue.

https://doi.org/10.1021/cbmi.4c00026
Chem. Biomed. Imaging 2024, 2, 490−500

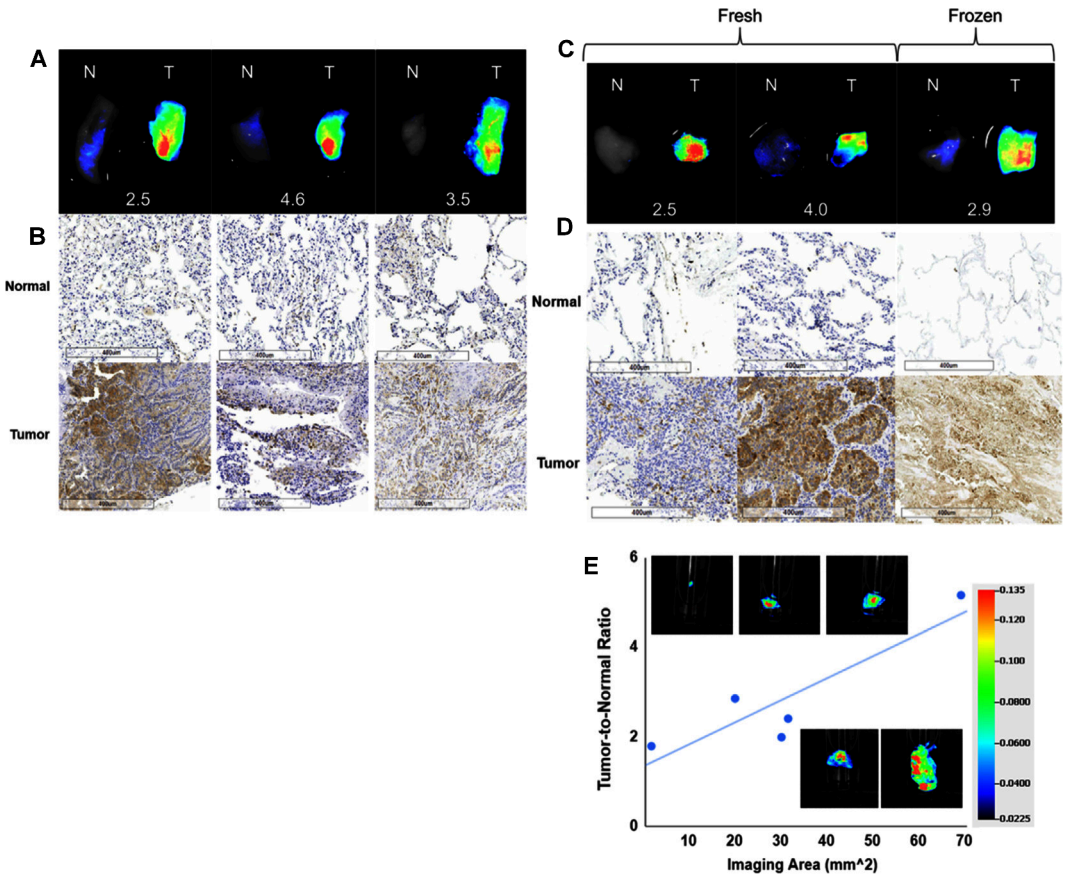

Figure 6. Activation of DDAO-A in NSCLC tissues. A. Fluorescence images of canine lung tumor (T) and normal lung (N) tissues (n = 3) 15 min after treating topically with 20 nmol of liposomal DDAO-A. Numbers represent the fluorescent TNR for each tissue. **B.** Histology of tissue from each tissue set with IHC for cPLA2 expression (brown). **C.** Representative fluorescence images of human lung tumor (T) and normal lung (N) tissues (n = 10) 15 min after treating topically with 20 nmol of DDAO-A. Numbers represent the fluorescent TNR for each tissue set. All tissue sets came from freshly resected specimens except one that had been frozen for 18 months at −80 °C. **D.** Histology of tissue from each tissue set with IHC for cPLA2 expression (brown). **E.** Limit-of-detection study for activated DDAO-A fluorescence. Serially dissected lung tumor tissue fluorescence was compared to normal lung tissue fluorescence from the same patient maintained at the same size. The resulting TNR was analyzed against imaging area. Tumor fluorescence was distinguishable from normal lung tissue fluorescence at imaging areas as small as 1.9 mm^2.

Table 2. Diagnostic Information for Canine Tissues

Sex	Age (yrs)	Diagnosis	Stage[a]	Baseline (TNR)	DDAO-A (TNR)
f	9	Squamous cell carcinoma	T1	1.8:1	2.5:1
f	6	Adenocarcinoma	T1	2.5:1	4.6:1
m	10	Bronchoalveolar carcinoma	T2	2.4:1	3.5:1

[a]Stage was determined using the TNM Classification of Malignant Tumors.

Table 3. Diagnostic Information for Human Tissues

Sex	Age (yrs)	Diagnosis	Stage[a]	DDAO-A (TNR)
M (n = 5)	66	Neuroendocrine	T1b	5.2:1
	76	Adenosquamous carcinoma	T3	4.1:1
	59	Adenocarcinoma	T3	4.0:1
	61	Adenocarcinoma	T1b	2.1:1
	75	Adenocarcinoma	T1a	1.8:1
F (n = 5)	65	Adenocarcinoma	T1b	2.9:1
	68	Adenocarcinoma	T2a	5.1:1
	60	Squamous cell carcinoma	T4	1.5:1
	66	Neuroendocrine, squamous cell, adenocarcinoma	T2b	2.0:1
	59	Carcinoid	T1a	2.5:1

[a]Stage was determined using the TNM Classification of Malignant Tumors.

Thus, DDAO-A could even be useful for identifying tumor tissues in cases where the specimens were not freshly acquired.

Histological analyses of the tissues showed qualitatively higher cPLA2 expression in tumor tissues in both canine and human tumors. Higher nuclear densities consistent with neoplastic tissues or tumor-associated inflammation were also observed by hematoxylin staining. Fluorescence imaging of the slides on the LI-COR Odyssey showed high DDAO fluorescence in tumor tissues and areas of high nuclear density in normal tissues suggesting probe activation in normal tissues was from tumor-associated inflammation or embedded micrometastases (Figures S10,S11). Thus, DDAO-A can be used to differentiate small residual tumor tissue from normal lung tissue. (Figures S10,S11). These images demonstrate that activated DDAO-A can be imaged after tissue fixation with higher fluorescence recorded in tumors and potentially in micrometastases or inflamed tissues. Further, the higher expression of cPLA2 observed in tumor tissues provides a basis for the mechanism of preferential activation of DDAO-A in tumors.

https://doi.org/10.1021/cbmi.4c00026
Chem. Biomed. Imaging 2024, 2, 490−500

A limit-of-detection study was conducted to determine the minimum tumor size that could be identified by DDAO fluorescence. TNRs remained above 2:1 for all tumor sizes except the smallest tissue (Figure 6E). At an imaging area of approximately 1.9 mm^2, the TNR was 1.9:1.

CONCLUSIONS

We demonstrated that DDAO-A is preferentially activated by lung cancer tissues *in vivo* and *ex vivo* in mouse models and canine and human tissue specimens. These data suggest DDAO-A is a promising candidate for translation to a veterinary clinical trial for back-table imaging and topical administration of DDAO-A in the surgical cavity to image residual lesions in canine patients with spontaneous NSCLCs. By utilizing canine and human patient tissues, we were able to minimize the number of animals required to validate our probe while demonstrating efficacy in spontaneous canine and human lung tumors. Thus, these data demonstrate the utility of *ex vivo* experiments as a reasonable substitute for *in vivo* experiments without compromising the impact of the research validating DDAO-A. Future work includes the synthesis of good laboratory practice (GLP) DDAO-A to transition the probe into canine clinical trials. DDAO-A may be useful in identifying positive tumor margins and guiding surgical procedures to improve rates of complete resections. However, systemic administration by intravenous injection will only be possible with further modifications to the nanoparticle formulation such as by the introduction of PEGylated lipids for improved probe retention time or formulation into micelles.

ASSOCIATED CONTENT

Supporting Information

The Supporting Information is available free of charge at https://pubs.acs.org/doi/10.1021/cbmi.4c00026.

Synthetic scheme of DDAO-A and DDAO-P; size distribution of DDAO-A-containing liposomes; lipid film stability studies; Western blot analysis of cPLA2 expression in TNBC and NSCLC cell lines; in vitro activation of DDAO-A in cells; fluorescence images of additional KLN 205 tumor-bearing mice treated with DDAO-A; baseline fluorescent images of canine tissues treated with JAS239; fluorescence and histology images for additional human tissue sets; hematoxylin-stained human tumor tissue and normal lung tissue with DDAO fluorescence (PDF)

AUTHOR INFORMATION

Corresponding Author

Edward J. Delikatny − *Department of Radiology, Perelman School of Medicine, University of Pennsylvania, Philadelphia, Pennsylvania 19104, United States*; Email: delikatn@pennmedicine.upenn.edu

Authors

Michael C. Hart − *Department of Radiology, Perelman School of Medicine, University of Pennsylvania, Philadelphia, Pennsylvania 19104, United States*

Ritesh K. Isuri − *Department of Radiology, Perelman School of Medicine, University of Pennsylvania, Philadelphia, Pennsylvania 19104, United States; Department of Chemistry, University of Pennsylvania, Philadelphia, Pennsylvania 19104, United States*; orcid.org/0009-0004-1710-6562

Drew Ramos − *Department of Radiology, Perelman School of Medicine, University of Pennsylvania, Philadelphia, Pennsylvania 19104, United States*

Sofya A. Osharovich − *Department of Radiology, Perelman School of Medicine, University of Pennsylvania, Philadelphia, Pennsylvania 19104, United States*

Andrea E. Rodriguez − *Department of Radiology, Perelman School of Medicine, University of Pennsylvania, Philadelphia, Pennsylvania 19104, United States*

Stefan Harmsen − *Department of Radiology, Perelman School of Medicine, University of Pennsylvania, Philadelphia, Pennsylvania 19104, United States*

Grace C. Dudek − *Department of Biology, University of Pennsylvania, Philadelphia, Pennsylvania 19104, United States*

Jennifer L. Huck − *Department of Clinical Studies, School of Veterinary Medicine, University of Pennsylvania, Philadelphia, Pennsylvania 19104, United States*

David E. Holt − *Department of Clinical Studies, School of Veterinary Medicine, University of Pennsylvania, Philadelphia, Pennsylvania 19104, United States*

Anatoliy V. Popov − *Department of Radiology, Perelman School of Medicine, University of Pennsylvania, Philadelphia, Pennsylvania 19104, United States*; orcid.org/0000-0002-4678-6307

Sunil Singhal − *Department of Surgery, University of Pennsylvania, Philadelphia, Pennsylvania 19104, United States*

Complete contact information is available at: https://pubs.acs.org/10.1021/cbmi.4c00026

Author Contributions

†M.C.H. and R.K.I. contributed equally to this work.

Notes

The authors declare no competing financial interest.

ACKNOWLEDGMENTS

This study was supported by the National Institutes of Health (NIH) R01 CA226412 (SS, EJD), R01 CA266234 (EJD, SS), P01 CA254859 (SS, EJD), and T32 GM008076 (MCH). Additional support came from R01 CA201328 (AVP) and the Transdisciplinary Awards Program in Translation Medicine and Therapeutics-Translational Biomedical Imaging Core (TAPITMAT-TBIC) pilot grants through UL1 RR024134 (EJD, SS, AVP). We would like to thank the Small Animal Imaging Facility in the Department of Radiology for use of the IVIS and LI-COR scanners and Comparative Pathology Core of the University of Pennsylvania School of Veterinary Medicine for help with immunohistochemistry as well as Lijun Luo and Drs. Andrew Tsourkas and Zhiliang Cheng of the University of Pennsylvania for help with liposomal formulations. TOC image was generated using ChemDraw, BioRender.com, and DALL-E 3.

REFERENCES

(1) *Cancer Facts & Figures*; American Cancer Society, 2022. https://www.cancer.org/research/cancer-facts-statistics/all-cancer-facts-figures/cancer-facts-figures-2022.html (accessed 2022).

(2) Majeed, U.; Manochakian, R.; Zhao, Y.; Lou, Y. Targeted therapy in advanced non-small cell lung cancer: current advances and future trends. *J. Hematol Oncol* **2021**, *14* (1), 108.
(3) Yang, D.; Liu, Y.; Bai, C.; Wang, X.; Powell, C. A. Epidemiology of lung cancer and lung cancer screening programs in China and the United States. *Cancer Lett.* **2020**, *468*, 82−87.
(4) Uramoto, H.; Tanaka, F. Recurrence after surgery in patients with NSCLC. *Transl Lung Cancer Res.* **2014**, *3* (4), 242−249.
(5) Kelsey, C. R.; Clough, R. W.; Marks, L. B. Local recurrence following initial resection of NSCLC: salvage is possible with radiation therapy. *Cancer J.* **2006**, *12* (4), 283−288.
(6) Slotman, B. J.; Lagerwaard, F. J.; Senan, S. 4D imaging for target definition in stereotactic radiotherapy for lung cancer. *Acta Oncol* **2006**, *45* (7), 966−972.
(7) D'Souza, A. V.; Lin, H.; Henderson, E. R.; Samkoe, K. S.; Pogue, B. W. Review of fluorescence guided surgery systems: identification of key performance capabilities beyond indocyanine green imaging. *J. Biomed Opt* **2016**, *21* (8), 080901.
(8) Holt, D.; Okusanya, O.; Judy, R.; Venegas, O.; Jiang, J.; DeJesus, E.; Eruslanov, E.; Quatromoni, J.; Bhojnagarwala, P.; Deshpande, C.; et al. Intraoperative near-infrared imaging can distinguish cancer from normal tissue but not inflammation. *PLoS One* **2014**, *9* (7), No. e103342.
(9) Wang, L. G.; Barth, C. W.; Kitts, C. H.; Mebrat, M. D.; Montano, A. R.; House, B. J.; McCoy, M. E.; Antaris, A. L.; Galvis, S. N.; McDowall, I. Near-infrared nerve-binding fluorophores for buried nerve tissue imaging. *Sci. Transl Med.* **2020**, *12* (542), 712 DOI: 10.1126/scitranslmed.aay0712.
(10) Tummers, Q. R.; Schepers, A.; Hamming, J. F.; Kievit, J.; Frangioni, J. V.; van de Velde, C. J.; Vahrmeijer, A. L. Intraoperative guidance in parathyroid surgery using near-infrared fluorescence imaging and low-dose Methylene Blue. *Surgery* **2015**, *158* (5), 1323−1330.
(11) Azari, F.; Zhang, K.; Kennedy, G. T.; Chang, A.; Nadeem, B.; Delikatny, E. J.; Singhal, S. Precision Surgery Guided by Intraoperative Molecular Imaging. *J. Nucl. Med.* **2022**, *63* (11), 1620−1627.
(12) Azari, F.; Kennedy, G.; Bernstein, E.; Delikatny, J.; Lee, J. Y. K.; Kucharczuk, J.; Low, P. S.; Singhal, S. Evaluation of OTL38-Generated Tumor-to-Background Ratio in Intraoperative Molecular Imaging-Guided Lung Cancer Resections. *Mol. Imaging Biol.* **2023**, *25* (1), 85−96.
(13) Keating, J.; Newton, A.; Venegas, O.; Nims, S.; Zeh, R.; Predina, J.; Deshpande, C.; Kucharczuk, J.; Nie, S.; Delikatny, E. J.; Singhal, S. Near-Infrared Intraoperative Molecular Imaging Can. Locate Metastases to the Lung. *Ann. Thorac Surg* **2017**, *103* (2), 390−398.
(14) Mondal, S. B.; Gao, S.; Zhu, N.; Liang, R.; Gruev, V.; Achilefu, S. Real-time fluorescence image-guided oncologic surgery. *Adv. Cancer Res.* **2014**, *124*, 171−211.
(15) Pogue, B. W.; Rosenthal, E. L.; Achilefu, S.; van Dam, G. M. Perspective review of what is needed for molecular-specific fluorescence-guided surgery. *J. Biomed Opt* **2018**, *23* (10), 1−9.
(16) Penet, M. F.; Mikhaylova, M.; Li, C.; Krishnamachary, B.; Glunde, K.; Pathak, A. P.; Bhujwalla, Z. M. Applications of molecular MRI and optical imaging in cancer. *Future Med. Chem.* **2010**, *2* (6), 975−988.
(17) Podo, F.; Bhujwalla, Z. M.; Iorio, E. Editorial: Exploring Cancer Metabolic Reprogramming through Molecular Imaging. *Front Oncol* **2017**, *7*, 79.
(18) Predina, J. D.; Newton, A. D.; Xia, L.; Corbett, C.; Connolly, C.; Shin, M.; Sulyok, L. F.; Litzky, L.; Deshpande, C.; Nie, S.; et al. An open label trial of folate receptor-targeted intraoperative molecular imaging to localize pulmonary squamous cell carcinomas. *Oncotarget* **2018**, *9* (17), 13517−13529.
(19) Ash, C.; Dubec, M.; Donne, K.; Bashford, T. Effect of wavelength and beam width on penetration in light-tissue interaction using computational methods. *Lasers Med. Sci.* **2017**, *32* (8), 1909−1918.
(20) Pansare, V.; Hejazi, S.; Faenza, W.; Prud'homme, R. K. Review of Long-Wavelength Optical and NIR Imaging Materials: Contrast Agents, Fluorophores and Multifunctional Nano Carriers. *Chem. Mater.* **2012**, *24* (5), 812−827.
(21) Hadjipanayis, C. G.; Stummer, W. 5-ALA and FDA approval for glioma surgery. *J. Neurooncol* **2019**, *141* (3), 479−486.
(22) Holt, D.; Singhal, S.; Selmic, L. E. Near-infrared imaging and optical coherence tomography for intraoperative visualization of tumors. *Vet Surg* **2020**, *49* (1), 33−43.
(23) Ogawa, M.; Kosaka, N.; Longmire, M. R.; Urano, Y.; Choyke, P. L.; Kobayashi, H. Fluorophore-quencher based activatable targeted optical probes for detecting in vivo cancer metastases. *Mol. Pharmaceutics* **2009**, *6* (2), 386−395.
(24) Rubtsova, N. I.; Hart, M. C.; Arroyo, A. D.; Osharovich, S. A.; Liebov, B. K.; Miller, J.; Yuan, M.; Cochran, J. M.; Chong, S.; Yodh, A. G.; et al. NIR Fluorescent Imaging and Photodynamic Therapy with a Novel Theranostic Phospholipid Probe for Triple-Negative Breast Cancer Cells. *Bioconjug Chem.* **2021**, *32* (8), 1852−1863.
(25) Mawn, T. M.; Popov, A. V.; Beardsley, N. J.; Stefflova, K.; Milkevitch, M.; Zheng, G.; Delikatny, E. J. In vivo detection of phospholipase C by enzyme-activated near-infrared probes. *Bioconjug Chem.* **2011**, *22* (12), 2434−2443.
(26) Popov, A. V.; Mawn, T. M.; Kim, S.; Zheng, G.; Delikatny, E. J. Design and synthesis of phospholipase C and A2-activatable near-infrared fluorescent smart probes. *Bioconjug Chem.* **2010**, *21* (10), 1724−1727.
(27) Faucher, F. F.; Liu, K. J.; Cosco, E. D.; Widen, J. C.; Sorger, J.; Guerra, M.; Bogyo, M. Protease Activated Probes for Real-Time Ratiometric Imaging of Solid Tumors. *ACS Cent Sci.* **2023**, *9* (5), 1059−1069.
(28) Walker, E.; Liu, Y.; Kim, I.; Biro, M.; Iyer, S. R.; Ezaldein, H.; Scott, J.; Merati, M.; Mistur, R.; Zhou, B.; et al. A Protease-Activated Fluorescent Probe Allows Rapid Visualization of Keratinocyte Carcinoma during Excision. *Cancer Res.* **2020**, *80* (10), 2045−2055.
(29) Weissleder, R.; Tung, C. H.; Mahmood, U.; Bogdanov, A., Jr In vivo imaging of tumors with protease-activated near-infrared fluorescent probes. *Nat. Biotechnol.* **1999**, *17* (4), 375−378.
(30) Chiorazzo, M. G.; Bloch, N. B.; Popov, A. V.; Delikatny, E. J. Synthesis and Evaluation of Cytosolic Phospholipase A(2) Activatable Fluorophores for Cancer Imaging. *Bioconjug Chem.* **2015**, *26* (12), 2360−2370.
(31) Chiorazzo, M. G.; Tunset, H. M.; Popov, A. V.; Johansen, B.; Moestue, S.; Delikatny, E. J. Detection and Differentiation of Breast Cancer Sub-Types using a cPLA2alpha Activatable Fluorophore. *Sci. Rep* **2019**, *9* (1), 6122.
(32) Tallman, K. R.; Beatty, K. E. Far-red fluorogenic probes for esterase and lipase detection. *Chembiochem* **2015**, *16* (1), 70−75.
(33) Tallman, K. R.; Levine, S. R.; Beatty, K. E. Profiling Esterases in Mycobacterium tuberculosis Using Far-Red Fluorogenic Substrates. *ACS Chem. Biol.* **2016**, *11* (7), 1810−1815.
(34) Kramer, R. M.; Sharp, J. D. Structure, function and regulation of Ca2+-sensitive cytosolic phospholipase A2 (cPLA2). *FEBS Lett.* **1997**, *410* (1), 49−53.
(35) Linkous, A. G.; Yazlovitskaya, E. M.; Hallahan, D. E. Cytosolic phospholipase A2 and lysophospholipids in tumor angiogenesis. *J. Natl. Cancer Inst* **2010**, *102* (18), 1398−1412.
(36) Geijsen, N.; Dijkers, P. F.; Lammers, J. J.; Koenderman, L.; Coffer, P. J. Cytokine-mediated cPLA(2) phosphorylation is regulated by multiple MAPK family members. *FEBS Lett.* **2000**, *471* (1), 83−88.
(37) Lin, C. C.; Lin, W. N.; Wang, W. J.; Sun, C. C.; Tung, W. H.; Wang, H. H.; Yang, C. M. Functional coupling expression of COX-2 and cPLA2 induced by ATP in rat vascular smooth muscle cells: role of ERK1/2, p38 MAPK, and NF-kappaB. *Cardiovasc. Res.* **2009**, *82* (3), 522−531.
(38) Kostarelos, K.; Emfietzoglou, D.; Papakostas, A.; Yang, W. H.; Ballangrud, A.; Sgouros, G. Binding and interstitial penetration of liposomes within avascular tumor spheroids. *Int. J. Cancer* **2004**, *112* (4), 713−721.

(39) Maruyama, K. Intracellular targeting delivery of liposomal drugs to solid tumors based on EPR effects. *Adv. Drug Deliv Rev.* **2011**, *63* (3), 161−169.
(40) van der Meel, R.; Fens, M. H.; Vader, P.; van Solinge, W. W.; Eniola-Adefeso, O.; Schiffelers, R. M. Extracellular vesicles as drug delivery systems: lessons from the liposome field. *J. Controlled Release* **2014**, *195*, 72−85.
(41) Smith, M. C.; Crist, R. M.; Clogston, J. D.; McNeil, S. E. Zeta potential: a case study of cationic, anionic, and neutral liposomes. *Anal Bioanal Chem.* **2017**, *409* (24), 5779−5787.
(42) Wang, M.; Herbst, R. S.; Boshoff, C. Toward personalized treatment approaches for non-small-cell lung cancer. *Nat. Med.* **2021**, *27* (8), 1345−1356.
(43) Yu, J. A.; Kalatardi, S.; Dohse, J.; Sadaria, M. R.; Meng, X.; Fullerton, D. A.; Weyant, M. J. Group IIa sPLA2 inhibition attenuates NF-kappaB activity and promotes apoptosis of lung cancer cells. *Anticancer Res.* **2012**, *32* (9), 3601−3607.
(44) Zhang, F. Y. L.; R, Z.; Li, J. X.; Fan, X. X.; Xie, C.; Liu, L.; Yao, X. J.; Leung, E. L. H. Phopsholipase A2 as a novel therapeutic target for in lung cancer. *Integr. Cancer Sci. Ther.* **2020**, *7*, 349.
(45) Batist, G.; Barton, J.; Chaikin, P.; Swenson, C.; Welles, L. Myocet (liposome-encapsulated doxorubicin citrate): a new approach in breast cancer therapy. *Expert Opin Pharmacother* **2002**, *3* (12), 1739−1751.
(46) Nakhaei, P.; Margiana, R.; Bokov, D. O.; Abdelbasset, W. K.; Jadidi Kouhbanani, M. A.; Varma, R. S.; Marofi, F.; Jarahian, M.; Beheshtkhoo, N. Liposomes: Structure, Biomedical Applications, and Stability Parameters With Emphasis on Cholesterol. *Front Bioeng Biotechnol* **2021**, *9*, No. 705886.
(47) Lucas, K. K.; Dennis, E. A. Distinguishing phospholipase A2 types in biological samples by employing group-specific assays in the presence of inhibitors. *Prostaglandins Other Lipid Mediat* **2005**, *77* (1−4), 235−248.
(48) Evans, J. H.; Spencer, D. M.; Zweifach, A.; Leslie, C. C. Intracellular calcium signals regulating cytosolic phospholipase A2 translocation to internal membranes. *J. Biol. Chem.* **2001**, *276* (32), 30150−30160.
(49) Nakamura, H.; Wakita, S.; Suganami, A.; Tamura, Y.; Hanada, K.; Murayama, T. Modulation of the activity of cytosolic phospholipase A2alpha (cPLA2alpha) by cellular sphingolipids and inhibition of cPLA2alpha by sphingomyelin. *J. Lipid Res.* **2010**, *51* (4), 720−728.
(50) Arlauckas, S. P.; Popov, A. V.; Delikatny, E. J. Direct inhibition of choline kinase by a near-infrared fluorescent carbocyanine. *Mol. Cancer Ther* **2014**, *13* (9), 2149−2158.
(51) Arlauckas, S. P.; Kumar, M.; Popov, A. V.; Poptani, H.; Delikatny, E. J. Near infrared fluorescent imaging of choline kinase alpha expression and inhibition in breast tumors. *Oncotarget* **2017**, *8* (10), 16518−16530.

https://doi.org/10.1021/cbmi.4c00026
Chem. Biomed. Imaging 2024, 2, 490−500